Chapter 5

1-D TiO_2 nanorods array-based sensor for selective and stable detection of VOCs

5. 1 Introduction

After a detailed discussion on gas sensing performance of TiO_2 nanotubes, in the current chapter, another highly ordered 1-D nanostructure of TiO_2 in the form of nanorods was considered for gas sensing application. TiO_2 nanostructures can be synthesized by using various techniques like sol-gel [1], spin coating [2], electrochemical anodization [3], thermal oxidation [4], and hydrothermal [5]. Out of these, hydrothermal method is a facile, low temperature, and cost-effective process to synthesize one dimensional (1-D) TiO_2 nanorods in rutile phase. TiO_2 nanorods can provide numerous porous sites for a faster diffusion of test vapors for gas sensing application whereas the rutile phase of TiO_2 may also offer a better stability to the sensor [6].

In the past, hydrothermally grown TiO_2 nanorods were reported by multiple researchers and these structures were generally grown on FTO/ITO glass substrates [7-11]. These substrates are proved to be less promising because of the following issues i.e. (i) challenges for device integration and compatibility, (ii) poor electronic properties, and (iii) less mechanical strength. Moreover, TiO_2 nanorods do not adhere very firmly on these glass substrates, and thus offers poor device stability.

In the present work, TiO_2 nanorods were grown on Ti substrate by optimizing the chemical and physical growth parameters of the hydrothermal method. Also, Ti substrate facilitates to fabricate a sandwich structure sensor device in which TiO_2 nanorods were sandwiched in between two parallel metal electrodes i.e. Ti substrate (bottom) and Au film (top). Afterward, 1-D TiO_2 nanorods based parallel electrode sensors were fabricated and tested in both resistive and capacitive modes at a very low

operating temperature (27-50 °C) for different volatile organic compounds (VOCs) like methanol, ethanol, acetone, 2-propanol, and benzene of concentrations in-between 50 to 300 ppm. In general, Au/TiO_2 nanorods/Ti sensor has two distinct advantages i.e. (i) 1-D barrier less electron transport with enhanced sensing performance [12] and (ii) suitability of a combined resistive and capacitive modes sensing with a single device [13]. In resistive mode, adsorption/desorption kinetics of target gas/vapor dominates the sensor sensitivity while in capacitive mode change in the dielectric medium of sensing layer in presence of VOC dominates the sensing mechanism. In this present endeavor, the performance of VOC sensor operating in both resistive and capacitive modes was studied and compared in terms of sensitivity, selectivity, and stability.

5. 2 Synthesis of TiO_2 nanorods by hydrothermal method

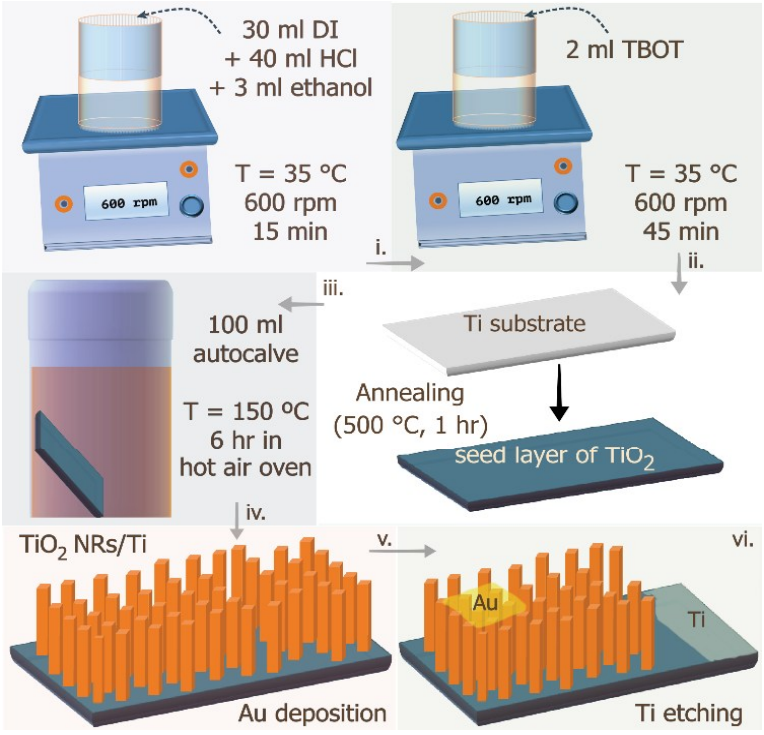

Fig. 5.1 Schematics showing sequence of the steps involved in fabricating Au/TiO_2 nanorods/Ti type sensor.

Ti metal foil was cut into dimensions of 1.5 cm × 1.5 cm and was cleaned with DI water followed by air ambient drying. Thermal oxidation of this Ti substrate at 500

°C in air ambient for 1 h resulted in the growth of a seed layer of TiO_2. For the synthesis of 1-D TiO_2 nanorods as a dominant structure, a chemical solution was prepared by maintaining a ratio of HCl and DI water as 30 ml and 40 ml, respectively. Afterward, 3 ml of ethanol was added to the solution and stirred for 15 min. Subsequently, 2 ml of titanium butoxide (TBOT) was added drop wise using a capillary tube and the resulting solution was vigorously stirred for another 45 mins to get a homogeneous solution. In the next step, the prepared solution was poured into a 100 ml autoclave (made of stainless steel) with Teflon liner. After this, thermally treated Ti foil was immersed in the solution at an angle of 45° with the horizontal plane of autoclave. The hydrothermal method was conducted by putting the autoclave in a hot oven for 6 h at 150 °C [14, 15]. After completion of hydrothermal process, autoclave was taken out and placed in air ambient (at room temperature) for 2 h. The autoclave was then opened up and the sample was taken out and rinsed with DI water. Fig. 5.1 (i.-v.) schematically shows the various steps involved in formation of TiO_2 nanorods on Ti substrate. After the successful formation of TiO_2 nanorods, the sample was annealed at 400 °C for 3 h for improving the crystallinity and mechanical strength of the as grown nanostructure. The morphological and structural details of the annealed samples were characterized by FESEM and XRD, respectively.

5. 3 Fabrication of TiO_2 nanorods-based sensor and experimental setup for VOC sensing

The fabrication technique for obtaining a sandwich structure sensor was similar to the steps discussed in sec. 2.2 (Chapter 2). However, there was a difference in geometrical dimensions of the sensor. TiO_2 nanorods/Ti samples were cut in dimensions of 3 mm × 7 mm and Au contacts were deposited through a Cu mask having an opening of 1 mm × 1 mm (Fig. 5.1 (vi)). The pressure of the vacuum chamber was maintained at ~10^{-6} mbar during Au deposition. Afterward, top right side of the TiO_2 sample was selectively etched by HF solution to obtain a bare Ti substrate of 1 mm × 3 mm, as

shown in Fig. 5.1 (vi.). A top contact of Au and a bottom contact of Ti were used as the electrodes of the sensor. Thus, the basic structure of the sensor was maintained similar to the previously discussed sensors based on TiO_2 nanotubes and only sensing material of the sensor was changed to TiO_2 nanorods

VOC sensing properties of the sensor were then evaluated in a static vapor sensing characterization system as discussed in sec. 3.2 (Chapter 3). The resistance and capacitance of the sensor were continuously recorded in the air as well as in VOC ambient at a sampling rate of 1 s. The operating temperature of the sensor was set at 50 °C by using a temperature-controlled heating mantle. The top lid of the glass chamber had a valve fitted orifice which acts as an outlet of the test vapor. VOCs of known concentration were injected into the glass chamber through the top orifice by using a micro-syringe. After obtaining the maximum changes in resistance and capacitance values of the sensor, the top lid valve was opened for the recovery of the sensor. During sensor characterizations, RH level and room temperature were maintained at ~40% and ~30 °C, respectively. Resistive response magnitude (RRM) and capacitive response magnitude (CRM) of the sensor were calculated following the eq. 2.7 and 2.8, respectively. Resistive selectivity coefficient (RSC) and capacitive selectivity coefficient (CSC) of the sensor for test vapor with respect to interfering vapor molecules were calculated using eq. 5.1 and 5.2, respectively and depicted as below:

$$\mathrm{RSC} = \frac{\text{RRM (test vapor)}}{\text{RRM (interfering vapor)}} \tag{5.1}$$

$$\mathrm{CSC} = \frac{\text{CRM (test vapor)}}{\text{CRM (interfering vapor)}} \tag{5.2}$$

Where, RRM (test vapor) and RRM (interfering vapor) are the resistive response magnitudes of the sensor for x ppm of test and x ppm of interfering vapor, respectively. In a similar manner, CRM (test vapor) and CRM (interfering vapor) are the capacitive response magnitudes of the sensor for x ppm of test and x ppm of interfering vapor, respectively.

5. 4 Characterizations of TiO_2 nanorods

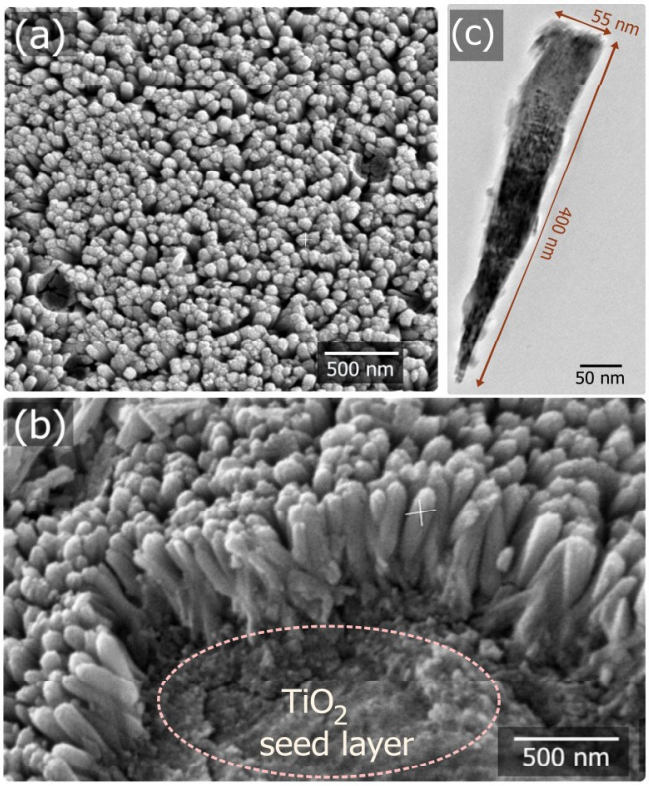

Fig. 5.2 (a) FESEM images of the annealed TiO_2 nanorods with top view, (b) side view; (c) TEM image of a single TiO_2 nanorods.

The surface morphology of TiO_2 nanorods was characterized by using a commercial FESEM as shown in Fig. 5.2 (a) and (b). Top view of the FESEM image shows that TiO_2 nanorods were grown uniformly on Ti substrate. During hydrothermal synthesis, TiO_2 nucleation starts in the form of nanorods and the entire growth of nanostructures was restricted to 1-D only due to the controlled reaction kinetics. Otherwise, a 3-D hierarchical nanoflowers could have been grown by self-organization of radially distributed nanorods [6]. Fig. 5.2 (b) shows the side view of the FESEM image composed of well-oriented 1-D TiO_2 nanorods only. From FESEM data, the average diameter and length of TiO_2 nanorods were found to be in the range of 30-50 nm and 350-500 nm, respectively. Fig. 5.2 (c) shows the TEM image of a single TiO_2 nanorod having length of 400 nm and thickness of 55 nm which further supports the FESEM results.

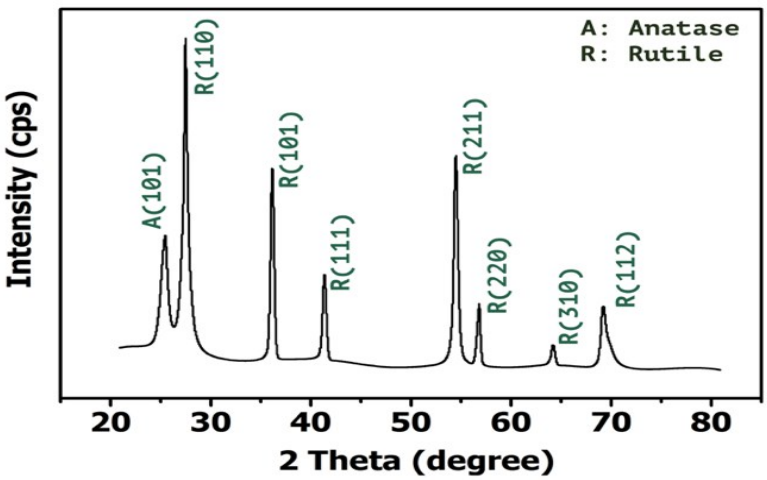

Fig. 5.3 XRD pattern of hydrothermally grown TiO_2 nanorods over Ti substrate.

Fig. 5.3 shows the X-ray diffraction peaks of the annealed TiO_2 nanorods sample where a sharp peak at 2ϑ value at 25.3° corresponds to (101) crystal plane of anatase phase (JCPDS No. 21-1272). Similarly, peaks at 2ϑ values of 27.4°, 36.09°,41.2°, 54.3°, 56.8°, 64.1°, and 69.4° correspond to (110), (101), (111), (211), (220), (310), and (112) crystal planes of rutile phases, respectively (JCPDS No. 21-1276). However, no XRD peak of Ti substrate was observed here which authenticates that the growth of TiO_2 layer over Ti substrate was uniform and sufficiently thick. Since, XRD spectra showed both phases of TiO_2 (anatase and rutile) and thus, their individual contents were calculated by using the Spurr's equation [9]. By measuring XRD peaks intensities of (101) and (110) planes of anatase and rutile, respectively, the percentage of anatase phase of TiO_2 was found to be 24.8% for the annealed sample. In addition, average crystalline sizes of TiO_2 anatase (101) and TiO_2 rutile (110) nano-clusters were calculated using Scherrer's formula and found to be 10.7 nm and 20.1 nm, respectively.

5. 5 VOC sensing characteristics of TiO_2 nanorods-based sensors

(a) I-V characteristics:

Fig. 5.4 shows the I-V characteristics of Au/TiO_2 nanorods/Ti parallel electrodes sensor operated at 50 °C in air and various concentrations of reducing vapor (methanol)

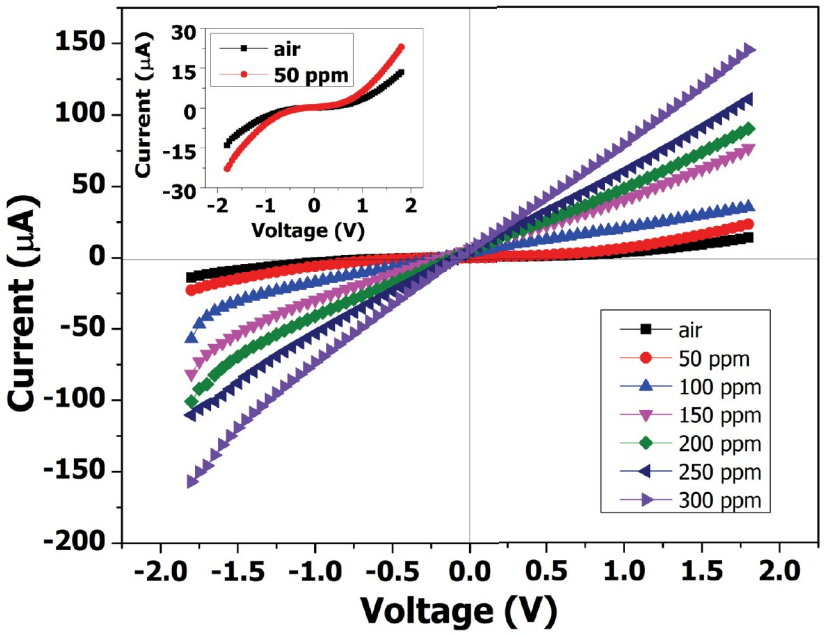

Fig. 5.4 I-V characteristics of Au/ TiO_2 nanorods/ Ti based sensor operated at 50 °C in air and different methanol concentrations.

ambient. I-V characteristics confirmed that the resistance of the sensor reduces with increase in concentration of methanol vapor, confirming an n- type behavior of TiO_2 nanorods. In addition, junctions of the sensor device exhibited a Schottky nature in air ambient. However, in methanol ambient, the sensor device tends to become ohmic in nature, showing a linear I-V characteristic. In air ambient, the porous surface of TiO_2 nanorods enhances the physisorption of oxygen molecules which become chemisorbed after consuming the free electrons available on n-type TiO_2 surface and remain in active states [16, 17]. As a result, a depletion region is formed on the surface of TiO_2 nanorods which is responsible for a higher series resistance as reflected in the I-V curve (in the inset of Fig. 5.4). Injected methanol vapor reacts with the active states of oxygen and gets oxidized. The oxidation of methanol results in the formation of aldehyde and free electrons are released which results in the decrease in depletion region as well as the junction series resistance. Depending upon the sensor ambient, methanol can be further oxidized to form the final products like CO_2 and H_2O, releasing free electrons [3]. Hence, the resistance of sensor decreases with increase of methanol concentration and the

device becomes ohmic in nature, as shown in Fig 5.4.

(b) Sensitivity:

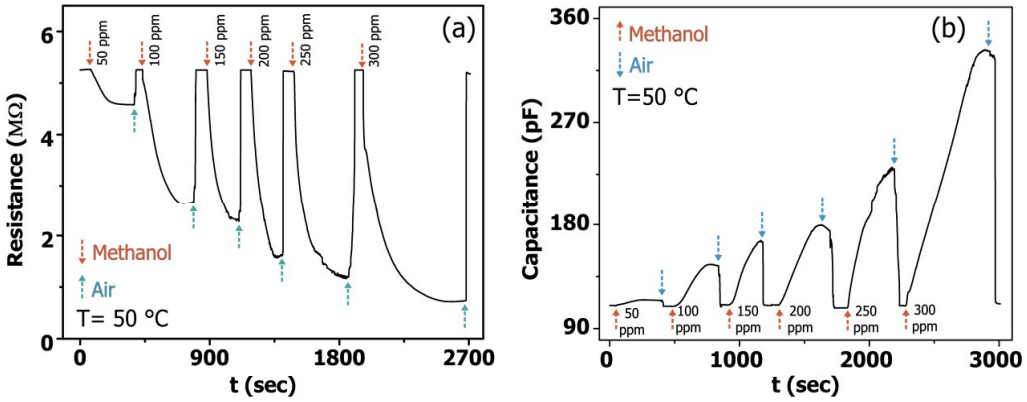

Fig. 5.5 Transient behavior of (a) the resistive change and (b) the capacitive change of the sensor when methanol concentration was increased from 50 ppm to 300 ppm.

Methanol sensing behavior of the TiO_2 nanorods sensor was tested for concentration ranging from 50-300 ppm, in an incremental step of 50 ppm. Initially, the resistance of sensor in air ambient, operating at 50 °C, was measured as approximately 5.3 MΩ. Upon exposure to 50 ppm of methanol vapor, resistance of the sensor was dropped abruptly to 4.6 MΩ. The resistance of the sensor was further reduced as the concentration of methanol vapor was increased stepwise from 50 ppm to 300 ppm. A typical transient behavior of resistive changes of the sensor towards different methanol concentrations is shown in Fig. 5.5 (a). It was found out that the resistive response was continuously increased with methanol vapor concentration and started to get saturate for the concentration of methanol above 300 ppm.

Fig. 5.5 (b) shows a transient behavior of capacitive changes of the sensor upon exposure to different concentrations of methanol vapor at 50 °C. Initially, the capacitance of the sensor in air ambient, operating at 50 °C, was measured to be approximately 109 pF. Upon exposure to 50 ppm of methanol vapor, capacitance of the sensor was marginally increased to 116 pF. However, the change of capacitance gets increased when the concentration of methanol vapor was stepwise increased from

50 ppm to 300 ppm. It was found out that capacitive change of the sensor was continuously increased with the concentration of methanol vapor and reached to 330 pF for 300 ppm of methanol concentration.

(c) Selectivity:

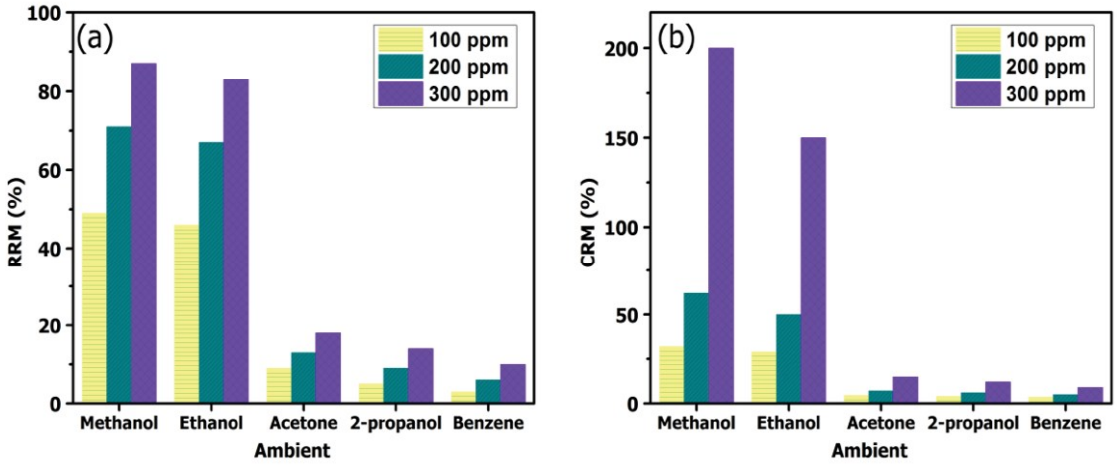

Fig. 5.6 (a) Resistive response magnitude (RRM) and (b) Capacitive response magnitude (CRM) of the sensor operating at 50 °C for 100, 200 and 300 ppm concentration of methanol, ethanol, acetone, 2-propanol and benzene.

In addition to resistive and capacitive responses of the sensor for various methanol concentrations, selectivity of the sensor was also examined by exposing sensor device to different VOCs ambient namely, methanol, ethanol, acetone, 2-propanol and benzene. The maximum change in resistance and capacitance values of the sensor for each VOC for concentrations of 100, 200 and 300 ppm were measured. RRM and CRM of the sensor are shown in Fig. 5.6 (a) and (b) respectively. Undoubtedly, sensor displayed the highest response magnitude towards methanol vapor for all concentration values, both in resistive and capacitive modes. However, the resistive and capacitive sensitivities of the sensor get decreased with the following sequence: methanol> ethanol> acetone> 2-propanol >benzene. Thus, the selectivity study envisaged that TiO_2 nanorods sensor was highly selective towards the methanol vapor as compared to other VOCs.

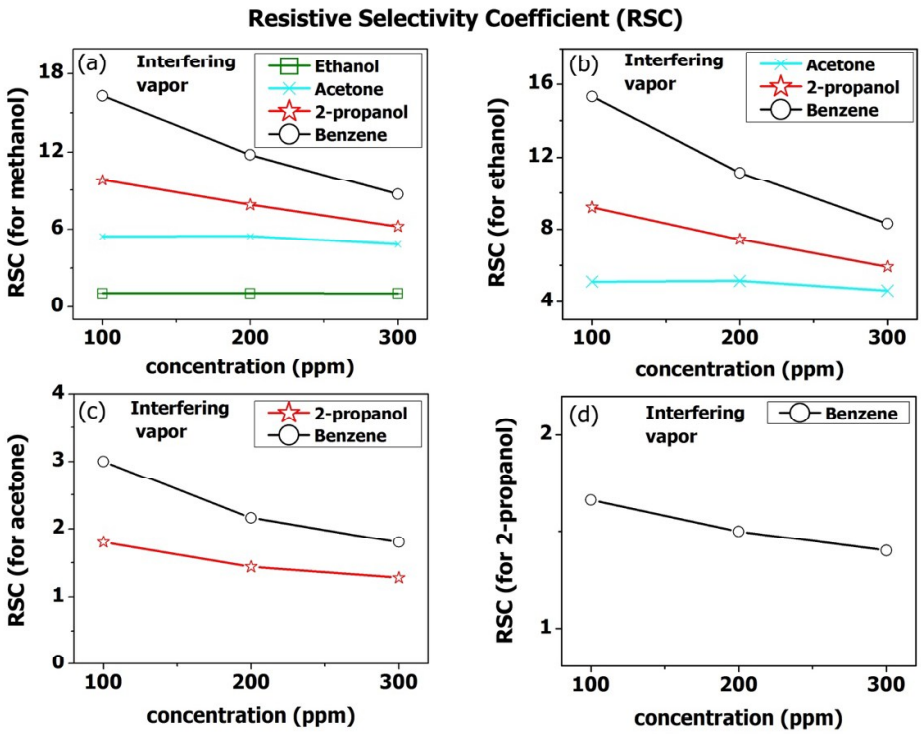

Fig. 5.7 Resistive selectivity coefficient (RSC) of the sensor for (a) methanol, (b) ethanol (c) acetone, and (d) 2-propanol.

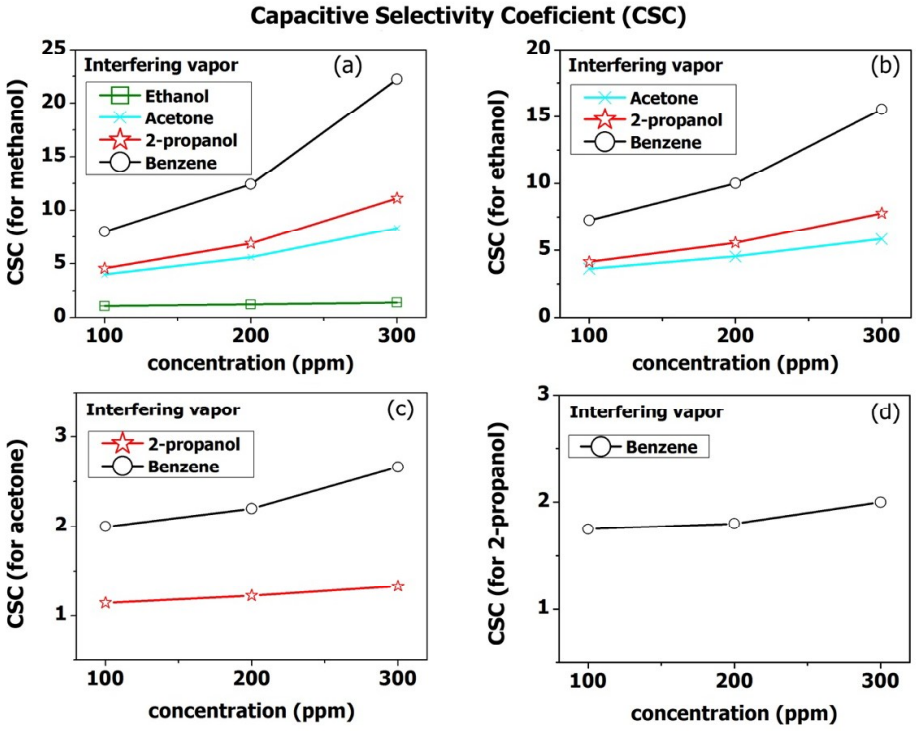

Fig. 5.8 Capacitive selectivity coefficient (CSC) of the sensor for (a) methanol, (b) ethanol (c) acetone, and (d) 2-propanol.

Resistive selectivity for any test vapor was found to be more at a lower concentration of VOCs and get decreased towards the higher concentration as seen in Fig. 5.7 (a)-(d). As an example (Fig. 5.7 (a)), the resistive selectivity coefficient (RSC) of the sensor towards the methanol vapor with respect to ethanol was measured as 1.06 for 100 ppm and decreased to 1.05 for 200 ppm and further to 1.04 for 300 ppm. In addition, the sensor displayed a maximum resistive selectivity coefficient (RSC=16.3)

towards 100 ppm of methanol vapor when 100 ppm benzene was considered as an interfering vapor. It has also been observed that the selectivity of the sensor in resistive mode was decreased with an increase in the concentration of a particular VOC.

In contrast to resistive selectivity, on the other hand, the sensor showed a less capacitive selectivity when the concentration of VOCs was less but it gets increased for higher concentrations of VOCs (Fig. 5.8 (a)-(d)). Capacitive selectivity of the sensor towards methanol vapor with respect to ethanol was found to be improved when concentrations of VOCs were increased. From Fig. 5.8 (a), capacitive selectivity coefficient (CSC) of the senor towards methanol with respect to ethanol was observed as 1.1, 1.24, 1.42 for concentrations of 100, 200, and 300 ppm, respectively. Thus, the sensor displayed better capacitive selectivity as compared to the resistive selectivity towards all concentration values of methanol when ethanol was present as an interfering vapor.

In this work, selectivity of the target vapor was compared with another interfering vapor. It was found out from the study that capacitive selectivity of the sensor is highly dependent on dielectric constant values of VOCs. The capacitive response was maximum for methanol as it exhibited maximum dielectric constant value (ε_r= 32.7) among all tested VOCs. Also, the capacitive response was minimum for benzene as it exhibited minimum dielectric value ε_r= 2-3) [18-19]. However, while comparing methanol selectivity with respect to ethanol, it was found that the sensor was more selective towards methanol in capacitive mode. Since, the dielectric constants

of methanol (ε_r= 32.7) and ethanol (ε_r= 24.7) are significantly different, the net change in capacitance value due to the variation in the dielectric medium of sensor was quite different for two VOCs and hence a better capacitive selectivity was achieved. Also, the sensor exhibited a less capacitive selective towards acetone with respect to 2-propanol as their dielectric constants (acetone ε_r= 20.7 and 2-propanol ε_r= 20.18) are marginally different which results in a similar change in capacitance. Thus, the sensor was unable to differentiate between these two VOCs.

From Fig. 5.7 and 5.8, resistive and capacitive selectivity of the sensor were compared with concentration (100-300 ppm) of different VOCs and the following outcomes were obtained: (i.) Resistive mode is more selective towards (a) methanol up to 150 ppm and 200 ppm for 2-propanol and benzene, respectively and (b) ethanol up to 168 ppm for 2-propanol and up to 212 ppm for benzene and capacitive mode become more selective beyond this concentration, (ii.) Capacitive mode is more selective towards (a) methanol with respect to ethanol and acetone and (b) ethanol with respect to acetone for all concentration ranges, and (iii.) Resistive mode is more selective towards (a) acetone with respect to 2-propanol and benzene and (b) 2-propanol with respect to benzene for all concentration ranges.

Resistive response of the sensor for a constant temperature predominantly depends on the number of adsorption sites available per unit surface area. As the concentration of target VOC increases, the number of adsorption sites get filled and hence the change in surface resistance starts to get saturate and finally results in saturation. This mechanism of RRM degrades the selectivity performance of the sensor in resistive mode for a higher concentration of VOCs. However, the capacitive response majorly depends upon the tracking of the change in dielectric properties of the medium (TiO_2 nanorods in this case) that exists between two electrodes of the sensor. However, in contrast with the resistive response which majorly depends upon effective surface area of nanorods, the capacitive response majorly depends upon both surface area of nanorods and volume of void regions in between nanorods. Thus, with an increase in

the concentration of VOCs, more void regions (air, $\varepsilon_r = 1$) get filled with VOCs ($\varepsilon_r > 1$) which results in the enhancement of dielectric constant value of the medium. Thus, capacitive response keeps on increasing with VOC concentration (till 300 ppm in this study) which enhances the selectivity performance of the sensor for higher concentration of VOCs. Overall, it can be concluded from the above studies that the resistive mode of operation is more preferable over the capacitive mode when concentrations of test and interfering vapors are small and capacitive mode exhibited a better selectivity when concentrations of both test and interfering vapors get increased.

(d) Stability:

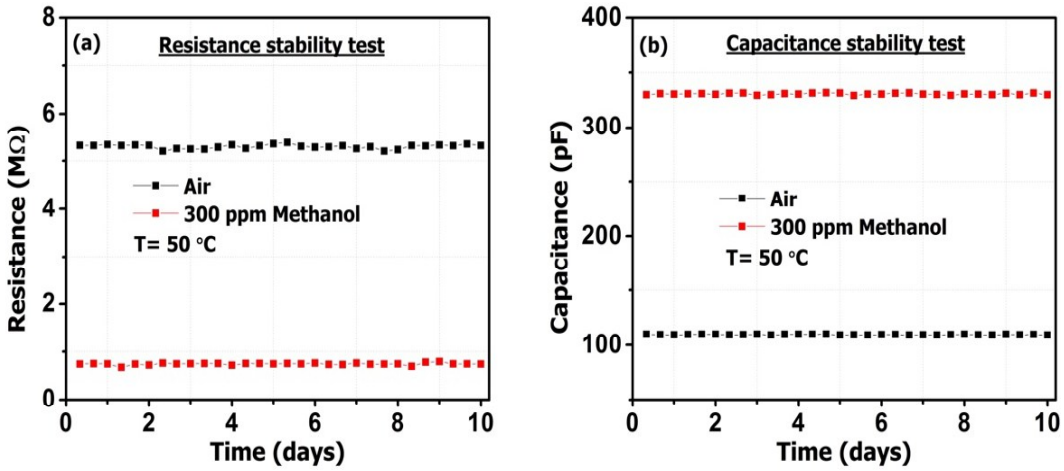

Fig. 5.9 Stability test of (a) resistance and (b) capacitance of TiO_2 nanorods sensor in air and 300 ppm methanol ambient.

Fig. 5.9 (a) and (b) show the stability tests of the sensor in air and 100 ppm methanol ambient, in terms of its resistance and capacitance values, respectively. The results showed good long-time stability for both modes. The average baseline value of resistance of sensor operating at 50 °C was found to be 5.39 MΩ with a standard deviation of ± 0.04 MΩ. Whereas, the average baseline value of the capacitance of sensor operating at 50 °C was found to be 109.4 pF with a standard deviation of ± 0.26 pF. As evident from XRD data, TiO_2 nanorods were in rutile phase (major) which

is the most stable phase of TiO_2 [20] and the sensor was operated at a relatively low temperature (50 °C) which results in better stability. Moreover, the TiO_2 nanorods were grown on a Ti substrate which offers a better lattice matching between the substrate and grown film which further enhances the mechanical stability of the sensor.

5. 6 Sensing mechanism of TiO_2 nanorods-based sensors

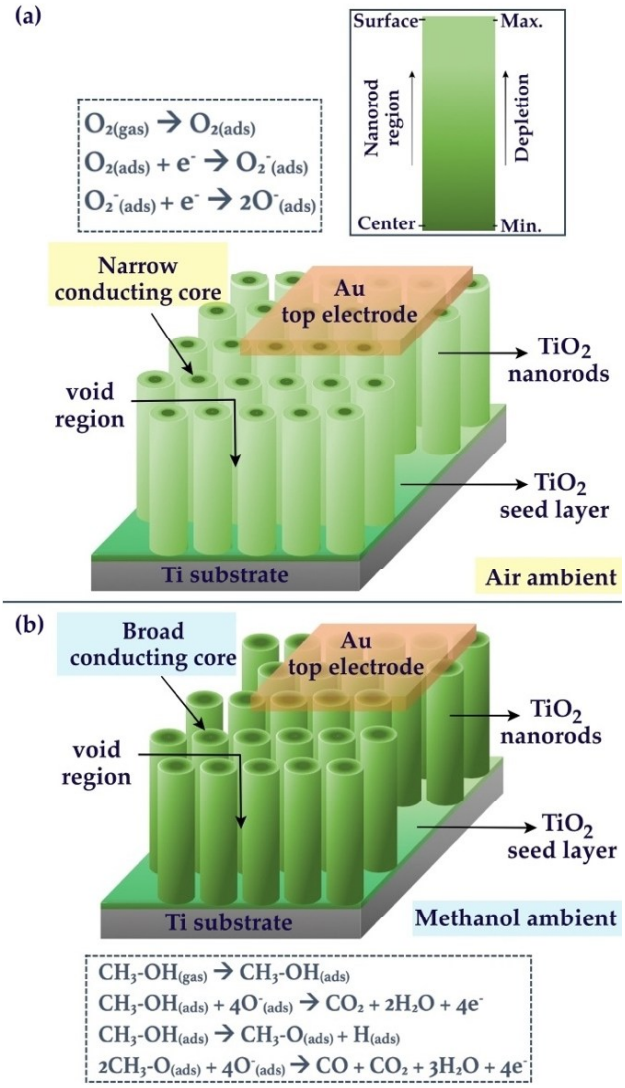

Fig. 5.10 A schematic of TiO_2 nanorods sensor with surface reactions related to the sensing mechanism (a) in air ambient and (b) in methanol ambient.

Transient behavior (in Fig. 5.5 (a) and (b)) of the sensor in resistive and capacitive mode is explained with a schematic shown in Fig. 5.10. In air ambient, oxygen species

like O_2^- and O^- get adsorbed on the surface of TiO_2 nanorods which result in capturing of free electrons. Therefore, the surface of TiO_2 nanorods gets depleted (Fig. 5.10 (a)) which is shown by a narrow conducting core region inside a nanorod that results in the increase in resistance between two parallel electrodes. However, in reducing VOC ambient like methanol, target VOC molecules react with these adsorbed oxygen ions and free electrons get released on TiO_2 surface. Thus, the conducting region of TiO_2 nanorods broadens up (Fig. 5.10 (b)) which reduces the resistance of sensor.

Space/volume between two parallel electrodes of the sensor typically compromised of TiO_2 nanorods and void regions as shown in Fig. 5.10 (a) and (b). Hence, the net capacitance of sensor can be considered as a parallel combination of two capacitances; one having TiO_2 nanorods as dielectric medium (C_{NR}) and other having void region/free space (C_F). In air ambient, C_F is small as the void regions in between two parallel electrodes have air as the dielectric medium. The capacitance of the device was measured to be less in air ambient as the dielectric constant of air is considered to be 1. However, in the presence of VOC like methanol, the void regions get started to fill and capacitance of the device starts to increase with VOC concentration as the dielectric constant of methanol is relatively higher (ε_r of methanol = 32.7) than that of air (ε_r= 1). The resistive change of the sensor was found to get saturated with increase in methanol concentration beyond 300 ppm as resistive sensitivity is restricted by finite surface area of TiO_2 nanorods. However, capacitive change of the sensor was found to keep on increasing with increase in methanol concentration beyond 300 ppm as capacitive change is governed by change in the dielectric medium of sensor between two electrodes of the sensor.

5. 7 Conclusions

In this work, a VOC sensor employing 1-D TiO_2 nanorods as an active layer grown over Ti substrate was fabricated using hydrothermal method. The direct growth of TiO_2 nanorods over the Ti substrate facilitates easy device integration, better stability,

low fabrication cost and placement of two electrodes in a vertical configuration. The sensor showed a high resistive and capacitive sensitivity towards methanol vapor at appreciably low operating temperature (50 °C) and low concentrations (50-300 ppm). The resistive response magnitude of 13-87 % and the capacitive response magnitude of 32-200 % were calculated upon exposure to 50-300 ppm of methanol vapor. Sensor showed better selectivity performance in resistive mode for lower ppm level of VOCs whereas capacitive mode showed better selectivity for higher VOCs concentration. Moreover, all these findings were explained by considering the surface free carrier concentration and dielectric properties of the sensor. Finally, the sensor showed excellent stability in terms of its baseline resistance and capacitance value where standard deviations of ± 0.04 MΩ for resistance and ± 0.26 pF for capacitance were observed. VOC sensing properties of TiO_2 nanotubes and nanorods were compared in terms of sensitivity, selectivity and stability in both resistive and capacitive modes. From all the above experimental results, methanol sensing data was compared for both TiO_2 nanotubes and nanorods. In general, it was found that RRM for both nanotubes and nanorods were similar but CRM for nanotubes was much higher than nanorods. Selectivity towards methanol with respect to ethanol was found to be better in nanotubes. The baseline resistance and capacitance values were found to be highly stable for both nanotubes and nanorods. Therefore, by analyzing all these parameters, TiO_2 nanotubes was chosen for developing a prototype of a selective VOC sensor.

References

1. M.A. Ponce, R. Parra, R. Savu, E. Joanni, P.R. Bueno, M. Cilense, J.A. Varela, M.S. Castro, Impedance spectroscopy analysis of TiO_2 thin film gas sensors obtained from water-based anatase colloids, Sensors and Actuators B 139 (2009) 447-452.
2. A. Nikfarjam, S. Hosseini, N. Salehifar, Fabrication of a highly sensitive single aligned TiO_2 and gold nanoparticle embedded TiO_2 nano-fiber gas sensor, ACS Appl. Mater. Interfaces 9 (2017) 15662-15671.

3. A. Hazra, B. Bhowmik, K. Dutta, P.P. Chattopadhyay, P. Bhattacharyya, Stoichiometry, length, and wall thickness optimization of TiO_2 nanotube array for efficient alcohol sensing, ACS Appl. Mater. Interfaces 7 (2015) 9336-9348.

4. A.Q.D. Faisal, Synthesis and characteristics study of TiO_2 nanowires and nanoflowers on FTO/glass and glass substrates via hydrothermal technique, J. Mater. Sci. Mater. Electron. 26 (2014) 317-321.

5. E. Hosono, S. Fujihara, H. Imai, I. Honma, I. Masaki, and H. Zhou, One-step synthesis of nano- micro chestnut TiO_2 with rutile nanopins on the microanatase octahedron, ACS Nano 1 (2007) 273-278.

6. Z.P. Tshabalala, K. Shingange, B.P. Dhonge, O.M. Ntwaeaborwa, G.H. Mhlongo, D.E. Motaung, Fabrication of ultra-high sensitive and selective CH_4 room temperature gas sensing of TiO_2 nanorods: Detailed study on the annealing temperature, Sensors and Actuators B 238 (2017) 402-419.

7. C. Cao, C. Hu, X. Wang, S. Wang, Y. Tian, H. Zhang, UV sensor based on TiO_2 nanorod arrays on FTO thin film, Sensors and Actuators B 156 (2011) 114-119.

8. Q. Mu, Y. Li, H. Wang, Q. Zhang, Self-organized TiO_2 nanorod arrays on glass substrate for self-cleaning antireflection coatings, J. Colloid Interface Sci. 365 (2012) 308-313.

9. S. Kumar, T. Vats, S. N. Sharma, and J. Kumar, Investigation of annealing effects on TiO_2 nanotubes synthesized by a hydrothermal method for hybrid solar cells, Optik 171 (2018) 492-500.

10. B. Liu and E.S. Aydil, Growth of Oriented Single-Crystalline Rutile TiO_2 nanorods on transparent conducting substrates for dye-sensitized solar cells, Sensors and Actuators B 9 (2009) 3985-3990.

11. E. Şennik, O. Alev, Z.Z. Öztürk, The effect of Pd on the H_2 and VOC sensing properties of TiO_2 nanorods, Sensors and Actuators B 229 (2016) 692-700.

12. A. Hazra, P. Bhattacharyya, Tailoring of the gas sensing performance of TiO_2 nanotubes by 1-D vertical electron transport technique, IEEE Trans. Electron Devices 61 (2014) 3483-3489.

13. K. Dutta, A. Hazra, P. Bhattacharyya, Ti/TiO_2 nanotube array/Ti capacitive device for non-polar aromatic hydrocarbon detection, IEEE Trans. Device and Materials Reliability

16 (2016) 235-242.

14. D. Tang, K. Cheng, W. Weng, C. Song, P. Du, G. Shen, G. Han, TiO_2 nanorod films grown on Si wafers by a nanodot-assisted hydrothermal growth, Thin Solid Films 519 (2011) 7644-7649.
15. H. Wang, Z. Chen, Y.H. Leung, C. Luan, C. Liu, Y. Tang, C. Yan, W. Zhang, J. A. Zapiena, I. Belloa, S. T. Lee, Hydrothermal synthesis of ordered single-crystalline rutile TiO_2 nanorod arrays on different substrates, Applied Physics Letters 96 (2010) 263104.
16. M. Lv, D. Zheng, M. Ye, J. Xiao, W. Guo, Y. Lai, L. Sun, C. Lin, J. Zuo, Optimized porous rutile TiO_2 nanorod arrays for enhancing the efficiency of dye-sensitized solar cells, Energy & Environmental Science 6 (2013) 1615-1622.
17. H.Y. Chen, T.L. Zhang, J. Fan, D.B. Kuang, C.Y. Su, Electrospun hierarchical TiO_2 nanorods with high porosity for efficient dye-sensitized solar cells, ACS Appl. Mater. Interfaces 5 (2013) 9205-9211.
18. E.S. Snow, F.K. Perkins, E.J. Houser, S.C. Badescu, T.L. Reinecke, Chemical detection with a single-walled carbon nanotube capacitor, Science 307 (2005) 1942-1945.
19. A. Hazra, A Physical Modeling of TiO_2 nanotube array-based capacitive vapor sensor, IEEE Trans. Nanotechnology 17 (2018) 93-99.
20. J. Bai, B. Zhou, Titanium dioxide nanomaterials for sensor applications, Chemical Reviews 114 (2014) 10131-10176.